Hall Effect Sensors Performance Investigation Using Three-Dimensional Simulations

Maria-Alexandra Paun, *Graduate Student Member, IEEE,* Jean-Michel Sallese, and Maher Kayal, *Member, IEEE*

***Abstract*—Several Hall effect sensors were modeled and evaluated regarding the Hall voltage and sensitivity using 3D physical simulations. For accurate results the numerical offset and its temperature drift were analyzed. The versatility of the simulation allows various Hall sensor implementations. The simulation procedure could guide the designer in choosing the Hall cell optimum fabrication process, shape and dimensions in terms of the performances envisaged to be achieved.**

***Index Terms*—Hall effect sensor, numerical offset/drift, 3D physical simulations**

I. Introduction

HALL effect sensors, based on magnetic phenomena, are one of the most commonly used sensing technologies today. Therefore these sensors are primarily employed as current sensors and serve many low-power applications like position sensing and contactless switching within automotive and industrial electronics [1].

The geometry plays an important role on the Hall effect sensors performance and was studied by the authors in [2]. A real Hall sensor has an offset due to geometrical errors, imperfections in the fabrication process, non-uniformity in material resistivity and thickness [3]. The offset and its temperature drift are important figures of merit in Hall sensors performance evaluation [4]. The offset is basically a parasitic voltage that adds to the Hall voltage.

The present paper analyzes the influence of the shape, dimensions, n-well doping concentration on the Hall effect sensors performances, including Hall voltage and sensitivity, with the aid of 3D physical simulations. In this sense, the study proposes a numerical estimation for Hall voltage and sensitivity with an analysis of numerical offset. We use three-dimensional numerical solutions to the system of partial differential equations governing galvanomagnetic carrier transport in magnetic-field-sensitive semiconductors, for optimal design of Hall effect sensors.

Section II presents the experimental data support, the basic physical model of the carrier transport in semiconductor materials and the methodology used for 3D structures simulation, introducing the design parameters for all proposed Hall cells. Section III is devoted to accurate prediction of both Hall voltage and sensitivity based on a comparative analysis of different Hall cell types. Consecutively its merit is to reveal which of the simulated sensors exhibited the best performance.

All the authors are with STI-IEL-Electronics Laboratory, Ecole Polytechnique Federale de Lausanne (EPFL), CH-1015 Lausanne, Switzerland *Corresponding author: M. A. Paun (e-mail: maria-alexandra.paun@epfl.ch).
Digital Object Identifier inserted by IEEE:

II. Methodology

A. Hall effect sensors experimental data support

In order to analyze the sensors performance an automated AC measurement procedure was previously developed and an experimental data basis was created. The testing system advantages are less noise, accuracy at lower frequencies and that the cells can be evaluated with a higher reliability under the same conditions. Several Hall effect sensors were integrated in 0.35 μm CMOS technology and evaluated for V_{HALL}, sensitivity, offset, etc. A part of the experimental results in conjunction with the geometry influence on the considered devices performance were presented in paper [2].

The offset analysis was of particular interest because in reality, Hall effect sensors have offset. The experimental data obtained for the offset at room temperature for different biasing currents is presented in Table I.

TABLE I
MEASURED STRUCTURES OFFSET (MV)

Hall cell	I=0.25mA	I=0.5mA	I=0.75mA	I=1mA
Basic	0.371	0.795	1.276	1.821
L	0.248	0.529	0.836	1.172
XL	0.033	0.091	0.167	0.258
Borderless	0.014	0.030	0.043	0.054

A first observation signals that there is an offset variance related to the particular sensors structures, which will be characterized in the modeling section.

The aim of the present study is to investigate the sensors performance including Hall voltage and sensitivity by three-dimensional physical simulations.

B. Hall effect sensors simulation

In semiconductor materials, the classical carrier transport models [5, 6] is based on the continuity equations

$$div\,\vec{J}_{nB} = q\left(R + \frac{dn}{dt}\right) \quad (1)$$

$$div\,\vec{J}_{pB} = -q\left(R + \frac{dp}{dt}\right) \quad (2)$$

where q is the elementary electronic charge, $\vec{J}_{nB}, \vec{J}_{pB}$ are magnetic field dependent current densities, R is the net recombination rate and n, p represent particle densities for electrons and holes, respectively. The particle densities expressions in terms of Fermi energy level $E_{F,n}$ and $E_{F,p}$ are

$$n = n_i \exp\left\{\frac{qV - E_{F,n}}{KT}\right\} \quad (3)$$

$$p = n_i \exp\left\{\frac{E_{F,p} - qV}{KT}\right\} \quad (4)$$

where V denotes the electrostatic potential, n_i is the intrinsic carrier concentration, T is the absolute temperature and k is the Boltzmann constant.

The differential equations (1) and (2) describe the conservation of electric charge and the carrier recombination rate can be a nonlinear function $R=R(V, n, p)$, in terms of V, n and p.

In particular, the transport models differ through the expressions used to define the current densities $\vec{J}_{nB}$ and $\vec{J}_{pB}$. For a complete description of semiconductor physical behavior, we also have to take into account the following equations

$$div(\varepsilon \vec{E}) = \rho \quad (5)$$

$$\vec{E} = -gradV \quad (6)$$

In the last two equations, $\vec{E}$ is the electric field, ε is the material electric permittivity and ρ is the space charge.

Replacing Eq. (4) in Eq. (3) and for a space charge ρ specified as $\rho = q(p - n + N)$ with $N = N_D - N_A$ denoting the fully ionized net impurity distribution, we get a partial differential equation of elliptic type

$$div(\varepsilon\, gradV) = -q(p - n + N) \quad (7)$$

The electrostatic potential V is the solution of the Poisson equation in (7).

We can mention that the magnetic induction effect manifests only in the definition relations of current density. In other words, the continuity equations (1) and (2) and the Poisson's equation (7) remain the same as well in the magnetic field absence.

In fact, for gaining insight into the operating principles of the final artifact, the distributions of electrostatic potential and current density in the device are fundamental. This allows one to determine optimal parameters of an ideal semiconductor structure.

3D Hall cells simulations were performed using Synopsys Sentaurus TCAD tool [7], which solves the Poisson equation, both electrons and holes continuity equations. A three-dimensional numerical modeling of carrier transport process in the magnetic field (electrostatic potential, current distributions) for semiconductor magnetic sensors with various geometries parameters is used.

The magnetic field acting on the semiconductor structure for Hall voltage generation was handled by the galvanic transport model. Mobility was considered via doping dependence formula and recombination processes were taken into account via Shockley-Read-Hall and Auger model. In this context, the ohmic contacts are assumed ideal and the contact regions support a sufficiently high dopant concentration. The carrier concentrations and electrostatic potential at the contact region are prescribed by the usual boundary conditions of Dirichlet type.

The 3D Hall cell mesh contained a sufficient number of points for a good tradeoff between accuracy and simulation run time. Small meshing dimensions and a high number of points increase the accuracy of the results, but take more CPU time and longer to execute. The mesh refinement window contained a mesh step between 0.1 and 1 μm on the three axes, resulting in a number of 5500 points for basic cell, 13000 points for borderless cell and 23000 for L and XL.

The meshed structure of one of the simulated Hall cell structures is presented in Fig. 1.

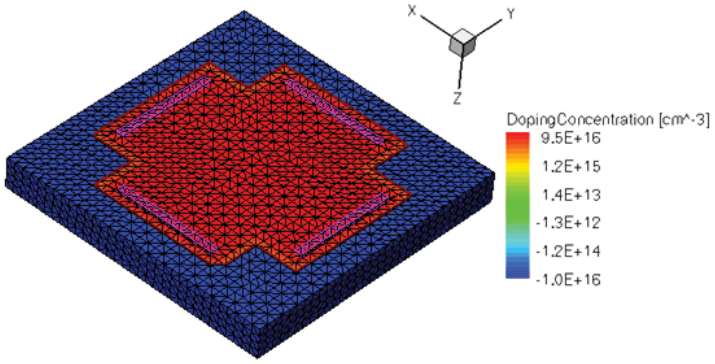

Fig. 1. The 3D model of basic Hall cell showing the doping concentration of all layers

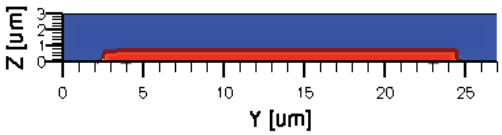

Fig. 2. An Ox cut showing the n-implantation on the p-substrate for basic Hall cell

C. *Hall effect sensors implementation*

Different 3D Hall effect sensor structures were modeled. In general these sensors are highly symmetric structures and invariant to a rotation of π/2. From the beginning all the cells were very accurately drawn, because any geometrical mismatch could significantly increase the offset and affect some future current-spinning techniques implementations.

Classical Greek-cross with progressive dimensions increase (resulting in basic, L, XL cells) and borderless cell were analyzed. The Hall cells were all modeled on a Silicon p-substrate with an n-well active region. All the implemented structures basically follow the same fabrication process, using a p-substrate with a Boron concentration of 10^{+16} cm^{-3} and an active n-well region doped with Arsenic of concentration 10^{+18} cm^{-3} (highly doped type) or 10^{+17} cm^{-3} (lightly doped type), in the form of a Gaussian profile implantation. The thickness is 3 μm for the p-substrate and 1 μm for the n-doped layer. The depletion layer formed under the p-n junction reduced the implantation depth to 0.7 μm for Greek cross cells.

In general, V_{HALL} is defined by the relation

$$V_{HALL} = \frac{Gr_H}{nqt} I_{bias} B \quad (8)$$

for a current polarization, or

$$V_{HALL} = G\mu_H \frac{W}{L} V_{bias} B \quad (9)$$

for a voltage polarization, respectively.

The sensitivity of Hall sensor is given by the relation

$$S_A = \frac{V_{HALL}}{B} = \frac{Gr_H}{nqt} I_{bias} \quad (10)$$

where B is the magnetic field induction, G is the geometrical correction factor, I_{bias} is the biasing current, r_H is the scattering factor of Silicon, usually 1.15, μ_H n is the Hall mobility and t is the thickness of the active region [3].

Since the V_{HALL} and therefore sensitivity are inversely proportional to the n-well doping concentration, a lightly doped n-well is normally used in the fabrication process. However, the two concentrations were analyzed.

To ensure a good simulation convergence, attention should be given to doping profile smoothing, so the abrupt edges were avoided at the p-n junction, by imposing a decay length of a hundred of nanometers.

For electrical tests purposes, each structure was equipped with four contacts, among which two are for biasing the device and the other two opposite ones for measurement purposes, by collecting the voltage drop.

L and W represent the cell length and width, respectively, while s stands for contact length. The width of the contacts is in general dictated by the technology used in the Hall cell fabrication process and in our simulations it was set at 0.7 µm. The distance from the contacts to the n-well borders is 0.9 µm all-around for basic and L cells, 0.3 µm and 0.95 µm for XL cell contacts to the top and sides of the active region respectively, and 14.9 µm for borderless cell. The position of contacts with respect to borders is important in the offset analysis as contour errors might increase it.

For each simulated Hall cell structure, the geometrical correction factor G was computed according to [3]. The resistance R is obtained by simulations for each cell.

The design details of all the four simulated Hall cell geometries are given in Table II.

TABLE II
SIMULATED HALL CELL STRUCTURES DESIGN PARAMETERS

Type of Hall cell	Basic	L	XL	Borderless
L (µm)	21.6	32.4	42.6	50
W (µm)	11.8	17.8	22.6	50
L/W	1.83	1.82	1.88	1
G	0.91	0.91	0.92	0.76
s (µm)	11	16	20.7	2.3
p-substate area (µm²)	729	1413.36	2361.96	3422.25
R (Ω)	482	489	589	1164

III. Results and Discussion

Simulations were performed on all the structures, using both voltage and current biasing, without and with magnetic field. The biasing current was considered from 0 to 1 mA or the biasing voltage from 0 to 1 V. The current biasing was finally chosen for simulations, being closer to the real situation.

Dimensions, via the geometrical correction factor as analyzed by authors in a recent paper [2], and distance between the contacts and the active region borders are important in the evaluation of the cells offset and sensitivity. The fourth analyzed shape, the borderless, has very small contacts and they are located more to the inside of the cell and far away from the n-well borders. This particular shape minimizes the influence of any errors that might appear on the borders.

The offset measurements were performed in the absence of magnetic field while for V_{HALL} and sensitivity estimation the magnetic induction was chosen at B=0.5 T. Nevertheless, different magnetic field intensities were simulated for V_{HALL} estimation.

The Hall voltage is affected by the offset by the relation

$$V_{out} = V_{HALL}(B) + V_{offset} \quad (11)$$

Even though the shapes are symmetric we obtain a non-zero offset, which will be referred to as numerical offset coming from the simulator. The Hall cells numerical offset was evaluated at room temperature and for certain temperatures in the interval between 0 and 100˚C. For highly doped n-well, the numerical offset drift was recorded at 8.41 µV/˚C for basic cell, 12.19 µV/˚C for L cell and 12.35 µV/˚C for XL cell.

Fig. 3 - Fig. 6 present the electrostatic potential for all simulated cells (highly doped n-well) for 1V biasing and no magnetic field. This situation is equivalent to the numerical offset analysis. The four electrical contacts used for biasing and measurement purposes are depicted as well. Imposing a certain voltage on electrode *a* will force a current to flow between *a* and *c* contacts. The offset and V_{HALL} are actually recorded as the voltage difference between the other two opposite contacts, *b* and *d* respectively.

Analyzing the simulations, we can easily observe the p-n junction, depicted by the brown thick line on the active region borders as well as the distribution of electric field lines in the absence of magnetic field. We can also see the effect of the contacts position with respect to the borders on the electrostatic potential lines distribution.

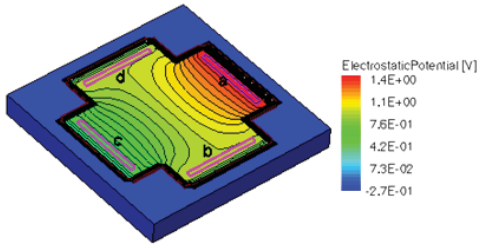

Fig. 3. Electrostatic potential for basic cell (highly doped n-well) for 1V biasing, B=0

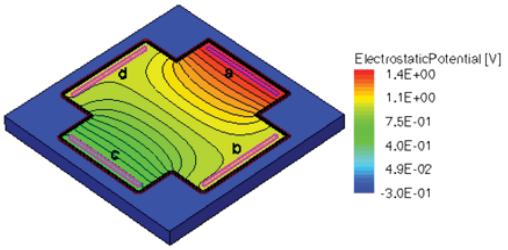

Fig. 4. Electrostatic potential for L cell (highly doped n-well) for 1V biasing, B=0

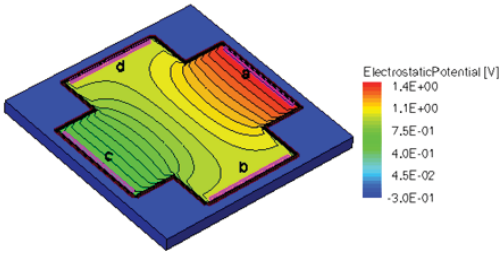

Fig. 5. Electrostatic potential for XL cell (highly doped n-well) for 1V biasing, B=0

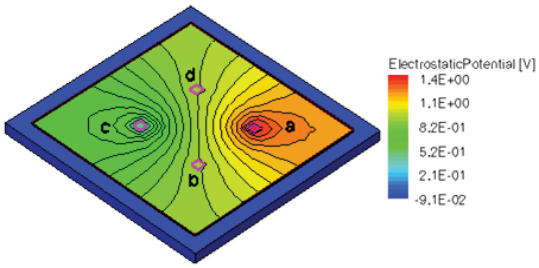

Fig. 6. Electrostatic potential for borderless cell (highly doped n-well) for 1V biasing, B=0

Regarding the room temperature numerical offset, the borderless cell displayed the minimum value, almost ten times lower than the classical Greek cross. Among the variations of Greek cross, the basic cell exhibited the lowest numerical offset, while the L and XL cells showed almost an equal offset.

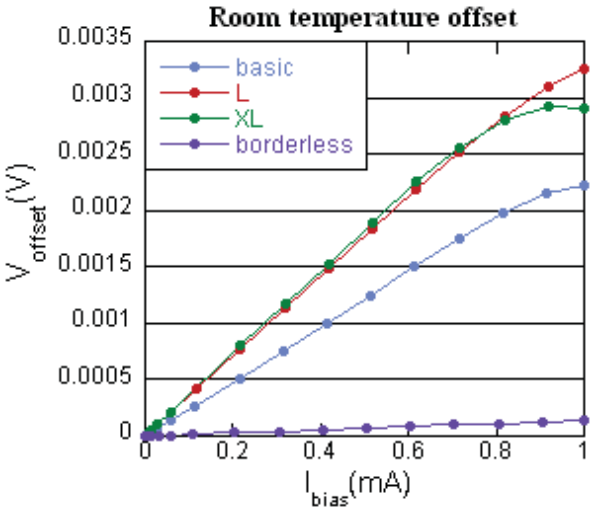

Fig. 7. Simulated V_{offset} (V) at room temperature for all cells (highly doped n-well)

Fig. 8 shows a lower offset for current biasing than when biasing with voltage in the case of the borderless cell. We can also observe that for the same borderless configuration, the cell with a lightly doped active region has a lower numerical offset than for the highly doped n-well case.

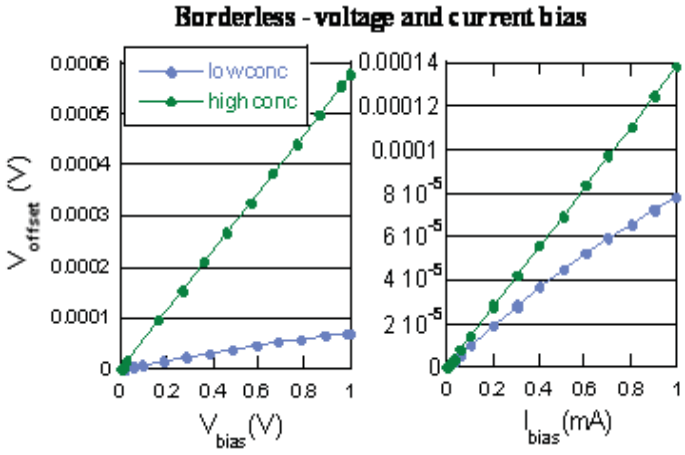

Fig. 8. Simulated V_{offset} (V) as a function of bias voltage and current for borderless cell (lightly and highly doped n-well)

The Greek cross cells, differing only in dimensions, preserved the same trend in numerical offset temperature behavior. While the basic cell exhibited the minimum numerical offset in this case, L and XL were very close in terms of the numerical offset, with a slightly less offset for XL cell. This analysis is very useful for accurate sensitivity drift estimations. The following figure presents the simulated numerical V_{offset}(V) vs. I_{bias} for basic cell taken for different temperatures within the interval 0 to 100˚C.

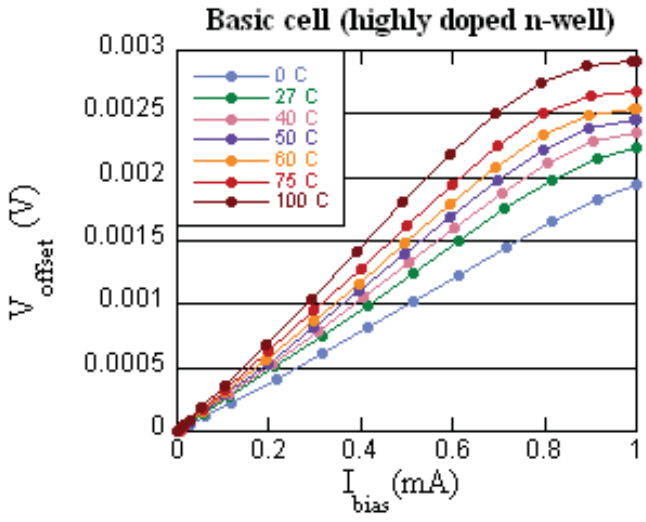

Fig. 9. V_{offset} (V) temperature behavior for basic cell

When applying a magnetic field of intensity B=0.5 T, the carriers deviate under the influence of Lorentz force. This situation emphasized by the distribution of the electric potential and the shape of the electric field lines can be easily observed in Fig. 10 - Fig. 13, recorded for a 1 V tension applied on the upper electrode.

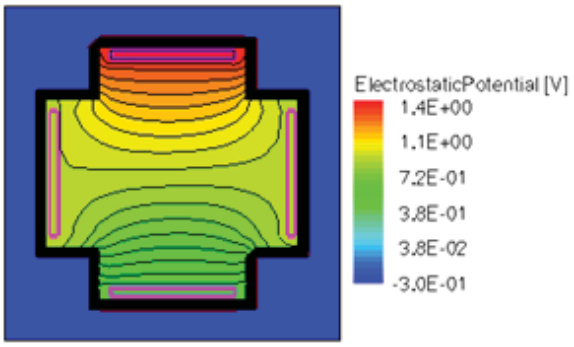

Fig. 10. Electrostatic potential for basic cell (lightly doped n-well) for 1V biasing, B=0.5 T

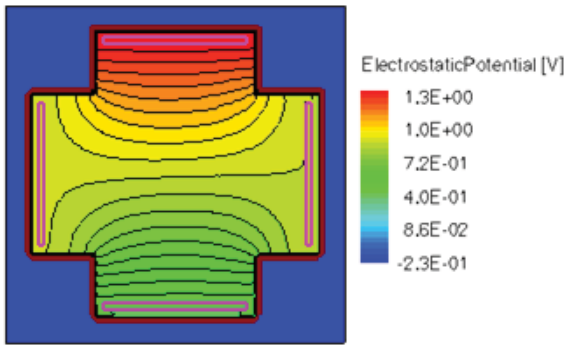

Fig. 11. Electrostatic potential for L cell (lightly doped n-well) for 1V biasing, B=0.5 T

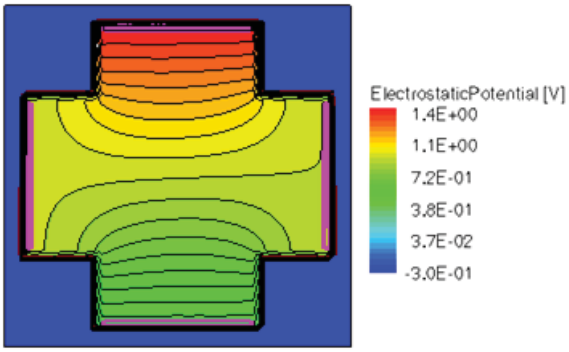

Fig. 12. Electrostatic potential for XL cell (lightly doped n-well) for 1V biasing, B=0.5 T

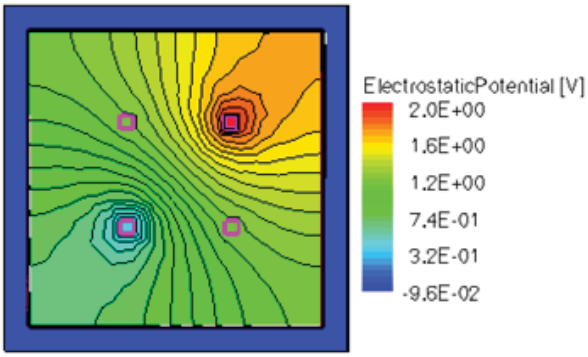

Fig. 13. Electrostatic potential for borderless cell (lightly doped n-well) for 1V biasing, B=0.5 T

For the proposed configurations (lightly doped n-well), V_{HALL} was simulated under the influence of magnetic field of B=0.5 T, for current biasing between 0 and 1 mA.

Taking into account the offset investigation previously presented, accurate information on V_{HALL} and sensitivity can be obtained. By consequence, the offset was subtracted from the total output voltage according to Eq. (11) and therefore V_{HALL} is presented in Fig. 14.

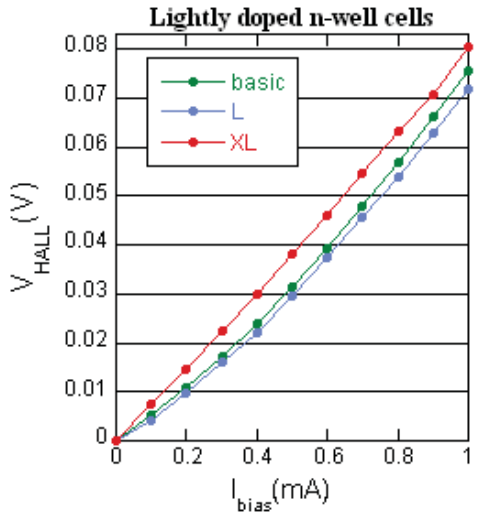

Fig. 14. Simulated V_{HALL} (V) vs. biasing current (lightly doped n-well) for B=0.5 T

For the borderless cell (lightly doped n-well), V_{HALL} was simulated for different magnetic field inductions, as we can see in Fig. 15.

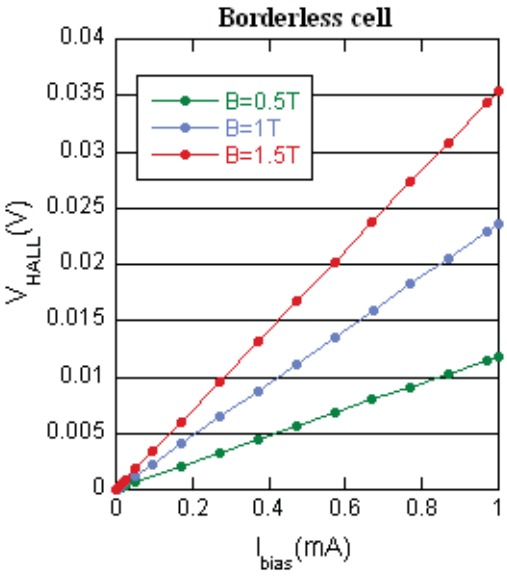

Fig. 15. Simulated V_{HALL} (V) vs. biasing current for borderless cell at different magnetic inductions

The numerical results previously reported for V_{HALL} are in good agreement with the experimental results [2], up to the extents of precise reproduction by simulation of the real structures tested.

As the offset is a parasitic voltage that adds to the total output voltage, we were interested to investigate the offset and

its temperature behavior in order to have accurate information for V_{HALL} and sensitivity. Normally, the offset should be zero for a simulated symmetric structure but the finite elements numerical computation, simulator's boundary conditions and meshing strategies might produce a non-zero offset in the absence of the magnetic field. For our simulations, meshes with higher number of point were also considered but the results were not significantly improved. For gaining accurate information on V_{HALL} and sensitivity we were interested to correctly investigate this numerical offset.

By dividing V_{HALL} to the magnetic induction we obtain the absolute sensitivity in V/T. Table III presents this information for all cells, in the lightly doped n-well case.

TABLE III
ABSOLUTE SENSITIVITY (V/T)

Hall cell	I=0.3mA	I=0.5mA	I=0.7mA	I=1mA
Basic	0.034	0.062	0.095	0.151
L	0.032	0.059	0.091	0.143
XL	0.045	0.076	0.109	0.161
Borderless	0.007	0.011	0.016	0.023

Among the Greek cross cells, the XL cell displayed the highest sensitivity. For the borderless cell the doping depth was higher than for the other shapes, therefore we expected a lower sensitivity according to Eq. (10), in this case almost five times less than for the other shapes.

IV. Conclusion

In order to analyze the influence of the shape, dimensions, n-well doping concentration on the Hall effect sensors performance, including V_{HALL} and sensitivity estimations 3D physical simulations using Synopsys Sentaurus TCAD tool were performed. The software allowed us to consider the magnetic field influence on semiconductors. Therefore, various Hall effect sensors following a certain fabrication process were modeled.

Moreover these results suggest an extrinsic offset evaluation in the future by observing the artificially induced offset effect on particular Hall sensor shapes. Also, (and to this purpose) a pertinent analysis of the intrinsic numerical offset generated by the simulator is to be taken into account to be able to distinguish between both offset causes.

Several Hall effect sensor configurations were simulated and evaluated for numerical offset, drift, V_{HALL} and sensitivity. In particular, the simulation and experimental results are in good agreement.

The simulation procedure could guide the designer in accurately estimating the V_{HALL} and sensitivity and lead to choosing the Hall cell optimum fabrication process, shape and dimensions in terms of the performances envisaged to be achieved.

Acknowledgment

This work has been supported by Swiss Innovation Promotion Agency CTI (Project 9591.1) and the company LEM SA – Geneva, Switzerland.

References

[1] E. Ramsden, "Hall-Effect Sensors – Theory and Applications", (2nd Edition), Elsevier, 2006

[2] M.A. Paun , J.M. Sallese, and M. Kayal, "Geometry influence on Hall effect devices performance", U.P.B. Sci. Bull., Series A, Vol. 72, Iss.4, 2010, p. 257-271

[3] R. S. Popovic, Hall Effect Devices, Second Edition, Institute of Physics Publising, 2004

[4] M. Kimura, Y. Yamaguchi, H. Hashimoto, M. Hirako,T. Yamaoka and S. Tania, "Analysis of Hall Voltage in Micro Poly-Si Hall Cells", Electrochemical and Solid-State Letters, 13(8), pp. J96-J98, 2010

[5] I. S. Selberherr, "Analysis and Simulation of Semiconductor Device", Vienna, Austria: Springer-Verlag, 1984

[6] W. Allegretto, A. Nathan, and H. Baltes, "Numerical Analysis of Magnetic-Field-Sensitive Bipolar Devices", IEEE Transactions On Computer-Aided Design, Vol. 10, No. 4, 1991

[7] Synopsys TCAD tools: http://www.synopsys.com/Tools/TCAD

Maria-Alexandra Paun received the Engineer Diploma from Politehnica University of Bucharest, Faculty of Engineering in Foreign Languages, Electrical Engineering Division, English Stream, with a major in Computer Science, graduating first of her promotion. The Master Project was made in the Electronics Laboratory at Ecole Polytechnique Fédérale de Lausanne (EPFL, Switzerland) and treated a subject in the field of low dropout voltage regulators. Between October 2008 and April 2009, she was awarded a postgraduate Marie Curie research fellowship at the University of Kent at Canterbury, UK, where she worked in the field of Optical Coherence Tomography. She is Assistant - Ph.D. student at EPF Lausanne working on the subject of Hall Effect sensors. Her main research interests are the analysis and modeling of sensors, development of circuit and three dimensional physical models. She is co-chair of IEEE Women in Engineering (WIE) Affinity Group in Switzerland. She has papers published in ISI journals and proceedings at national and international conferences. The paper from MIXDES 2011 Conference is recipient of the "Poland Section IEEE ED Chapter Special Award".

Jean-Michel Sallese received the MSc degree from the Institut National des Sciences Appliquées (France) and the Ph.D in physics from the University/CNRS of Nice-Sophia Antipolis (France) where he worked on deep levels characterization in semiconductors. He joined the Swiss Federal Institute of Technology in Lausanne (EPFL) in 1991 where he worked on semiconductor laser diodes characterization and modeling. He is currently giving lectures on advanced semiconductor devices as and his research activities focus on compact modeling of multigate MOSFET's as well as modeling of Micro-Electro-Mechanical Systems.

Maher Kayal received the M.S. and Ph.D. degrees in electrical engineering from the Ecole Polytechnique Fédérale de Lausanne (EPFL, Switzerland) in 1983 and 1989 respectively. He has been with the Electronics laboratories of the Ecole Polytechnique Fédérale de Lausanne (EPFL, Switzerland) since 1990, where he is currently a professor and vice dean for education of the school of engineering. He has published many scientific papers, is coauthor of three text books dedicated to mixed-mode CMOS design and he holds seven patents. His technical contributions have been in the area of analog and Mixed-signal circuits design including highly linear and tunable sensor microsystems, signal processing and CAD tools for analog design and layout automation. M. Kayal is a recipient of the Swiss Ascom award in 1990 for the best work in telecommunication fields. He is author and co-author of the following paper award in: ED&TC conference in 1997, IEEE-AQTR in 2006, Mixdes conference in 2007 & 2009, Powertech conference in 2009. M. Kayal received in 2009 the Swiss credit award for best teaching.